The Report Committee for Agatha Karen Bennett
Certifies that this is the approved version of the following report:

The Design of Anti-Reflective Coatings for a Quantum Cascade Laser Emitting Light in the Mid-Infrared Range

APPROVED BY
SUPERVISING COMMITTEE:

Supervisor: _____
Richard Crawford

Co-Supervisor: _____
Mikhail Belkin

The Design of Anti-Reflective Coatings for a Quantum Cascade Laser Emitting Light in the Mid-Infrared Range

by

Agatha Karen Bennett, B.S.

Report

Presented to the Faculty of the Graduate School of

The University of Texas at Austin

in Partial Fulfillment

of the Requirements

for the Degree of

Master of Arts

The University of Texas at Austin

August 2013

Dedication

To Bruce, Justin and Sydnee,

whose love and encouragement made this work possible.

Acknowledgements

Many thanks to Dr. David Allen and Dr. Richard Crawford for all they have done to make me a better teacher. Their wit and wisdom has inspired me beyond measure.

A special thanks goes to Theresa Dobbs, the face and voice of the MASEE program, who always made sure we "dotted our *i*'s and crossed our *t*'s." She is my hero.

Thank you Cohort 3, for making this experience so fun. Going to class was never a chore.

I would also like to thank Dr. Mikhail Belkin for the chance to learn something new. It was incredibly generous of him to open up his lab to me. It is an experience that I will never forget.

I am eternally grateful to Yifan Jiang, one of Dr. Belkin's graduate students, for her time and expertise. I cannot begin to pay her back for everything she has done to help me through my research, so I only hope to pay it forward.

Abstract

The Design of Anti-Reflective Coatings for a Quantum Cascade Laser Emitting Light in the Mid-Infrared Range

Agatha Karen Bennett, M.A.

The University of Texas at Austin, 2013

Supervisor: Richard Crawford

Co-Supervisor: Mikhail Belkin

Quantum cascade lasers (QCL) are semiconductor lasers that emit radiation in the mid-infrared to the terahertz (THz) range. External cavity quantum cascade lasers are broadly tunable mid-infrared and even THz laser sources that have a wide variety of applications in spectroscopy, sensing, imaging and other areas. Anti-reflection (AR) coatings, when applied on the laser facet reduce parasitic lasing, increase spectrum purity and tuning range, are crucial for good performance of external cavity systems. This report describes the process of determining the thickness of a double layer AR coating, applying the coatings to a quantum cascade laser and testing its reflectivity in the mid-infrared range. We determined the thickness of each layer of the AR coatings by building a propagation matrix model using Mathematica. We applied the coatings of Al_2O_3 and ZnSe using an Electron Beam Physical Vapor Deposition and a Sputtering Deposition system. Finally we tested the reflectivity of the laser by measuring a change in threshold current. The initial reflectivity of 30% was reduced to 7.7% with the addition of the AR coatings.

Table of Contents

List of Figures

Chapter 1: Introduction

Photonics, the study of light, is a new field of physics and engineering that specializes in the emissions, transmissions and sensing of light. Its roots began with the MASER, microwave laser, invented in the 1950's but saw record growth in the '80's due to the expansion of telecommunications. After the "dot-com" crash in 2001, photonics diversified and other areas of light application benefitted from the new technology. Advancements in science, engineering and manufacturing processes furthered the development of light technology. Today, light applications such as lasers, LED and fiber optics are ubiquitous.

Some of the advancements in this fast growing field are being made at the Microelectronics Research Center in Austin, TX. Directed by Dr. Mikhail Belkin, his research group utilizes quantum cascade lasers (QCL) to generate mid-infrared (Mid-IR) and terahertz (THz) beams. This frequency range corresponds to wavelengths several micrometers (μm) to hundreds of μm long, which is highly desired for spectroscope-based imaging and other applications. The first THz QCL was demonstrated in 2001 in Italy (Williams, 2007); however, THz QCL still requires cryogenic cooling and has a limited tuning range, making them impractical for commercial use. Belkin's group uses intra-cavity difference frequency generation (DFG) QCL to generate THz radiation which has the advantage of generating this wavelength at room temperature, and it also has a broad tuning range over 1.7 to 5.257 THz (Vijayraghavan, 2013). The device still has some hurdles to overcome, such as increasing the output power, but continual progress is being made.

Anti-reflection (AR) coating is a critical technology to generate single-mode tunable THz sources. The purpose of this research is to design, fabricate and test an

AR coating that will work in the Mid-IR range. Following the introduction, this paper will briefly describe appropriate literature about laser technology, the design and set-up of the experiment, its results and, perhaps, most importantly, how the information gained in this research will improve teaching practices in science and engineering.

Chapter 2: Literature Review

STIMULATED EMISSIONS AND LASERS

When a photon, a 'particle' of light interacts with an atom, the photon's energy can be absorbed. This energy, measured in electron volts (eV) is expressed in the following equation:

$$E = hf = \frac{hc}{\lambda}$$

where E is the energy, h is Plank's constant and f is the frequency of the light wave in hertz (Hz), c is the speed of light and λ is the wavelength of the light. If the photon has the energy, $hf = E_2\text{-}E_1$, where E_2 and E_1 are corresponding electron energy levels (see Figure 1) conservation of energy dictates that an electron will move to a higher energy level. Eventually, the electron will move to a more stable energy level and a photon with the same energy is emitted. A photon can stimulate the emission of another photon, only if the photon has the precise amount of energy and the electron is already in the exited state. The photon must carry the same amount of energy needed for the electron to take the quantum jump needed in absorption. The excited electron drops down to a lower energy level, releasing two photons with the same frequency and in the same phase. This is the basis for all lasers. It differs from all other light sources in that it is monochromatic and produces a narrow beam of light (Knight, 2012, Kasap, 2006).

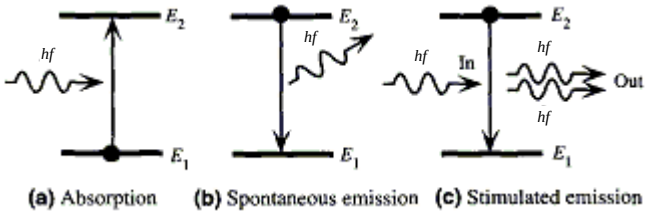

Figure 1: Interactions of light with matter. The energy of the photon, *hf*, is equal to E2-E1. (Kasap, 2006)

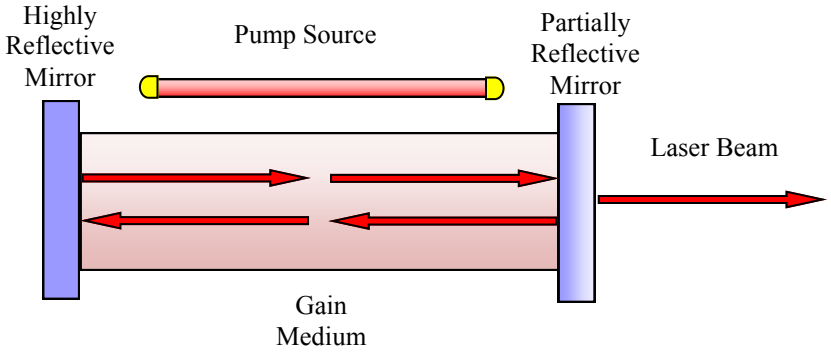

Figure 2: Components of a Laser

All lasers employ similar strategies in order to lase. Before energy is applied, most atoms within the gain medium are likely at their ground state, the position where electrons are most stable, N1>>N2. However, in order for lasing to occur, energy must be added, to excite most of the atoms. The process of exciting the atoms to a higher energy state is called "pumping." When more atoms are in an excited state than there are in the ground state, N2>>N1, it is called the "population inversion." Photons of the correct frequency are incident on the excited atoms and stimulate the emissions of photons that have the same frequency, phase and amplitude. The light reflects from the mirrors and travels back and forth within the medium, causing more light to be emitted from excited electrons. Some light is allowed through the partially reflective mirror forming the characteristic laser beam (Knight, 2012, Kasap, 2006).

DIODE LASERS

Scientists and engineers utilized the same laser principles, applied them to semiconductors and in 1962, produced the first laser diode, a small gallium-arsenide crystal that emitted infrared light. It could only operate with current pulses less than a millisecond and needed to be cryogenically cooled, but nevertheless, its small size

promised many new applications (Hayashi, 1984). Semiconductor lasers generate light by sending a current through the active region between the "p-n junction." Atoms with three valence electrons, such as boron, aluminum and gallium are added to the p-type material in a process called doping, creating the positive charge carrier, the "holes." The excess electrons in the n-type semiconductor, the negative charge carrier, are produced by doping with phosphorous, antimony or arsenic, atoms with five valence electrons (Nave, 2013). When the two materials are combined, electrons flow from the conduction band, made of the n-type semiconductor, to the holes in the valance band, made of the p-type semiconductor. This momentary diffusion of electrons creates a third region, the depletion region or the energy band gap (Kasap, 2006).

When current is applied, an incoming photon can stimulate electrons in the conduction band to recombine with the holes in the valence band. The interband transition of electrons generates a photon that has energy equal to that of the energy band gap. The energy band gap makes up the active region of the laser. The n-p layers have different refraction indices and therefore, confine the stimulated light to the active region.

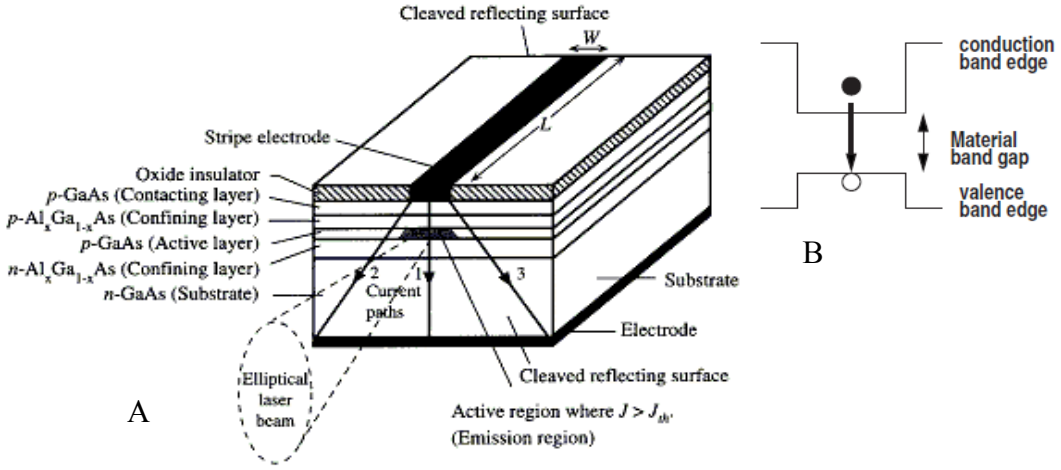

Figure 3: A) The structure of a double heterojunction laser diode (Kasap, 2006).
B) An interband transition of a diode laser. (Chakraborty, 2003)

The cleaved faces of the semiconductor provide the reflecting surfaces and the band gap of the material determines the wavelength produced (Kasap, 2006). Most laser diodes emit light in the visible to the mid-infrared range, depending on their structure and material.

QUANTUM CASCADE LASERS

Quantum cascade lasers (QCL) were first demonstrated in 1994 by Jèrôme Faist, Federico Capasso and their team at Bell Labs (1994). Unlike diode lasers, which generate radiation through electron-hole pair recombination, Faist, et al. (1994) used intersubband transitions in repeated stacks of semiconductor quantum well heterostructures to create these unique light sources that generate mid-infrared to far-infrared radiation. The first QCL had much room for improvement; operating with a low efficiency and requiring cryogenic cooling. However, QCL sparked the imaginations of many engineers and have since undergone a rapid evolution of improvements in design (Yao, 2012) and new applications for its use continue its rapid development (Williams, 2007).

As their name implies, QCL employ quantum mechanics to generate light. The active region of the laser is made of many layers of "intersubband transitions in multiple-

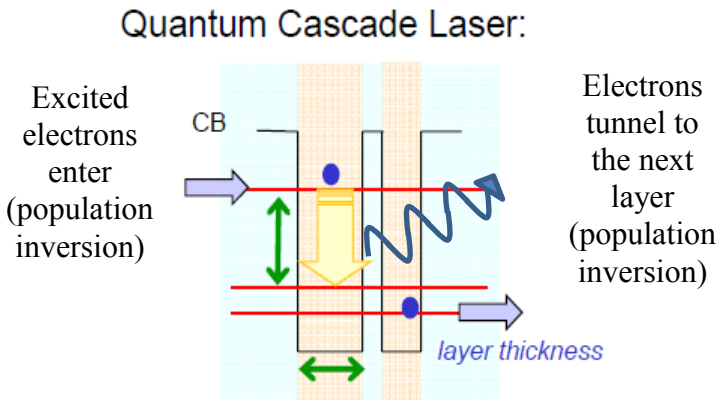

Figure 4. Conduction-band diagram for QCL (Gmachl, 2005)

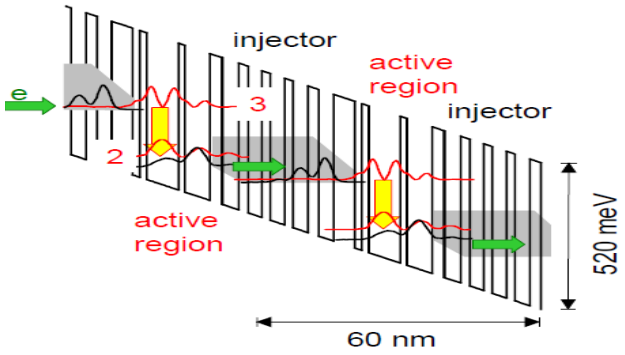

Figure 5. Quantum cascade at optimal voltage (Gmachl, 2005)

quantum well structures" (Yau, 2012). When excited electrons drop down quantum wells, they release photons with the corresponding energy, shown in Fig 3 (Gmachl, 2005). Electrons that drop, tunnel to the next layer and begin another population inversion. This is the "cascade" from which its name is derived.

Whereas the materials that make up a semiconductor diode laser limit its properties, QCL's are limited by their engineering. More than one diode laser is needed to generate multiple colors; however, with band-structure engineering, QCL's can generate various wavelengths of light (Gmachl, 2005). These layers of engineered bands are grown by molecular-beam epitaxy to produce microns-thick layers of semiconductor crystals. (Faist, 1994, Williams, 2007). With the right voltage, the active region will take on the staircase shape seen in Fig.4. The electrons cascade through the layers amplifying the radiation. Waveguide cladding provides optical confinement, allowing the light to generate parallel to the layers (Faist, 1994).

Although diode lasers are widely used in near-infrared optical communication, they can scarcely reach above the 4μm mid-infrared range. The band structure engineering of the QCL effectively covers the mid-infrared range, from approximately 4μm-12μm, and recent advancements and novel techniques produced

radiation in the THz range. Applications such as imaging, spectroscopy, sensing of toxic gases and explosives exploit the uniquely engineered QCL (Williams, 2007).

TUNABLE LASERS

QCL have the added advantage of being tunable. Continuous tuning can be achieved with a distributed feedback (DFB) QCL by changing the heat sink temperature. This causes a change in the refractive index of the laser waveguide (Gmachl, 2005, Yau, 2012). External cavity (EC) lasers employ external optical components, such as mirrors or diffraction gratings, to complete their optical resonator. EC QCL can also be tuned using the Littrow configuration, see figure 6. In this arrangement the diffraction grating is used for coarse tuning (Maulini, 2006,Yau, 2012) of the laser. The grating is angled precisely so that the first-order diffraction goes back into the laser. Only the wavelength satisfying the Bragg diffraction condition will be amplified, while other wavelengths will have sufficiently large losses and cannot be stimulated. Either the zeroth-order diffraction or emissions from the other facets of the QCL supply the output beam. Fine tuning of the

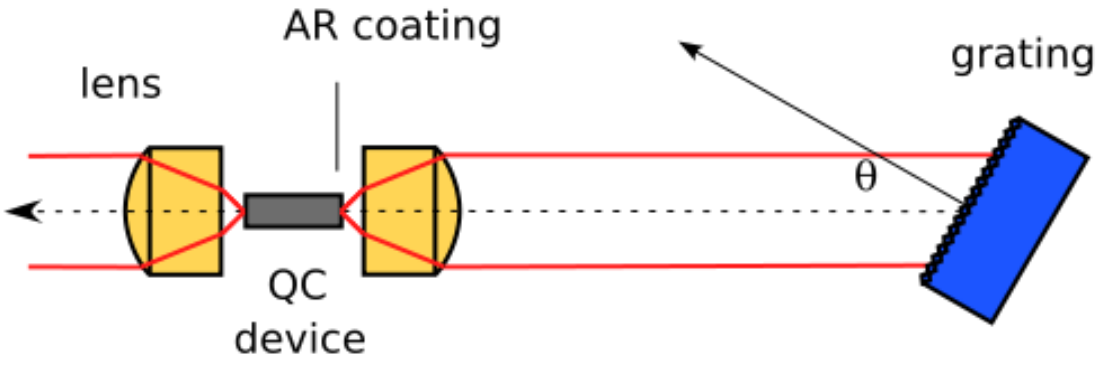

Figure 6: Littrow configuration of an EC QCL. In this arrangement, the cleaved surface of the front facet provides the partially reflective mirror. The AR coating with zero reflectivity allows the radiation to transmit unimpeded to the diffraction grating which provides the other mirror of the resonator cavity (Weida, 2008).

laser requires both changing the grazing angle and varying the heat sink temperature (Maulini, 2006).

ANTI-REFLECTIVE COATING

Both the DFB and EC QC lasers require anti-reflective (AR) coatings for efficient operations. Distributed feedback lasers require AR coatings to reduce self-lasing (Yau, 2012). External cavity QC lasers employ AR coatings to suppress multiple feedback from the laser facet and thereby increasing the tuning range (Maulini, 2006).

Anti-reflective coatings employ the principle of destructive interference to reduce reflection and are often used on optical devices to improve performance (see Figure 7). AR coatings on solar panels, for instance, improve transmittance of light optimizing power. Augustin-Jean Fresnel first modeled the mathematics of reflection and refraction of light incident on a surface. For a thin film on a substrate, the refractive index of an AR coating is found to be, $n = \sqrt{n_{air} n_s}$; where n_s is the refractive index of the substrate and, n_{air} is air's refractive index. When the $n^2 = n_s$ condition is met, a λ/4 layer is used but only if a single AR coating is used. Double AR coatings, also called v- coatings due to their

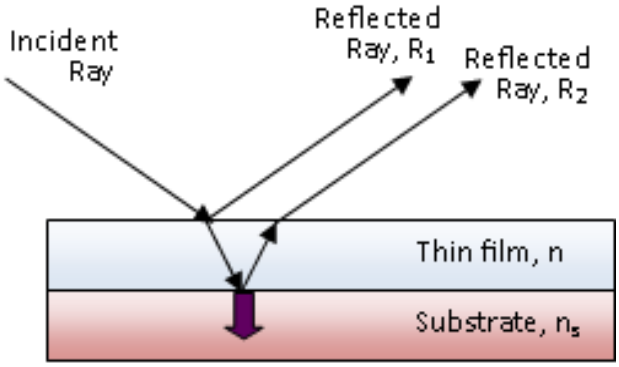

Figure 7: Interference. If ray 1 undergoes complete destructive interference with ray 2, they would cancel each other out and there would be no reflection.

V-shaped graphs, are used to further reduce reflectance and good choices for lasers since they work extremely well at specific wavelengths. Other methods used to achieve zero reflectivity include gradually lowering the refractive index in a multilayer structure and changing the surface topography like the structure of a moth's eye (Raut, 2011).

Having the right refractive index is not the only requirement for an ARC. Some materials, such as ZnS, ZnSe, YF_3 and CeF_3 are opaque to visible light but are transparent in the Mid IR range. In addition to transparency for the needed wavelength, the coating must be robust; so as to handle the wear and tear of use, and be able to adhere to the substrate. Maulini (2006) tried ZnS as an option. It has low loss in Mid-IR range and a refractive index of 2.2, but it does not adhere well to the QCL facet and chipped off easily. found that a single layer of AR coating, ZnS, did not work well with their EC QCL. They instead used a double layer AR coating consisting of YF_3 and ZnS because the YF_3 bonded to the QCL facet well, while the ZnS joined to the YF_3. The double layer structure had low reflectivity in the 3 to 12μm range (Maulini, 2006).

Chapter 3: Research Methods

CALCULATING REFLECTANCE OF A DOUBLE LAYER ANTI-REFLECTION COATING

An AR coating is essential to the design of an external cavity lasers, boosting its performance by diminishing the amount of reflective light. For minimal reflection, the reflected waves must superimpose and undergo destructive interference. The ideal solution for zero reflectance is to use a λ/4 layer, or odd number multiple of it, with a material that has an index of refraction of $n = \sqrt{n_s}$. In our case, the laser has an index of refraction of n_s= 3.2, therefore n≈1.8. As there is no unknown material with a refractive index of 1.8 that is transparent in the mid-infrared range, an alternate solution was needed.

Double layer AR coatings can be used for zero reflectance at specific wavelengths. Minimal reflection can be achieved with a double layer AR coating, λ/4 thick, if the two materials have refractive indices that conform to the condition $n_1^2 n_{sub} = n_2^2 n_{air}$. Unfortunately, AR coatings that fit those conditions could not be found, either. Nonetheless, zero reflectance can still be achieved by reducing impedance mismatching (Raut, 2011). This is feasible if the refractive index of n_1<1.8 and n_2>1.8. This increases the material options as long as they remain transparent in the mid-infrared range.

Here, we used Maulini's (2006) model to calculate the thicknesses of each layer of the double layer AR coating. Imagine an electromagnetic wave propagating along the z-axis in a medium as shown in Figure 8. Maxwell's equations for a plane wave with no charges, $\rho=0$, and no currents, $J=0$, are expressed by:

$$\nabla \cdot \mathbf{E} = 0 \qquad \nabla \times \mathbf{E} + \frac{\partial \mathbf{B}}{\partial t} = 0$$

$$\nabla \cdot \mathbf{B} = 0 \qquad \nabla \times \mathbf{B} - \frac{n^2}{c^2}\frac{\partial \mathbf{E}}{\partial t} = 0 \qquad (3.1)$$

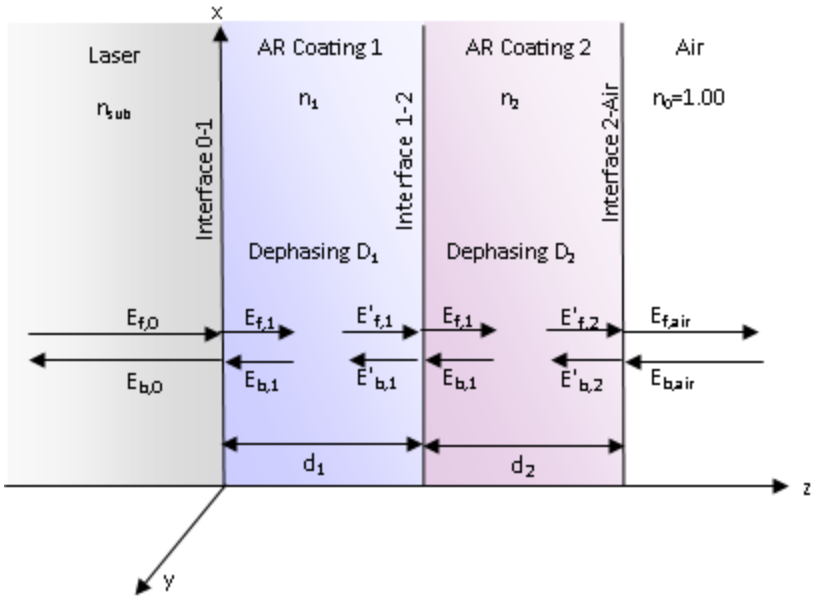

Figure 8. Model of the AR coating on a laser substrate. Incident light is polarized in the x-direction moving in the z-direction from left to right.

The electric and magnetic fields that generate the monochromatic and polarized light in the laser are shown as (Maulini, 2006),

$$E_0(\mathbf{x},\mathrm{t}) = \left[E_{f,0} e^{ik_0 z} + E_{b,0} e^{-ik_0 z} \right] e^{-i\omega t}$$

$$B_0(\mathbf{y},t) = \left[\frac{n_0 E_{f,0}}{c} e^{ik_0 z} - \frac{n_0 E_{b,0}}{c} e^{-ik_0 z} \right] e^{-i\omega t} \qquad 3.2$$

The light strikes "interface 0-1," the boundary between the laser and the first layer of the AR coating at normal incidence. Some light passes into the AR coating, while a fraction of the light reflects back. The boundary conditions are given by "The Fresnel Equations." By matching the electric and magnetic fields at the boundary we get

$$\tau_{01} = \frac{2n_{sub}}{n_{sub} + n_1}$$

$$\rho_{01} = \frac{n_{sub} - n_1}{n_{sub} + n_1} \qquad 3.3$$

where τ_{01} and $\rho 01$ are the transmission and reflection coefficients, respectively (Orfanidis, 2002). The index of refraction may be a complex number where $n_{sub}=n_{R+i}n_I$ and in_I relates to the absorption coefficient, $\alpha = \frac{4\pi n_I}{\lambda}$ (Maulini, 2006). The forward and backward electric fields at the laser/AR coating interface are related by the matching matrix:

$$\begin{pmatrix} E_{f,0} \\ E_{b,0} \end{pmatrix} = \frac{1}{\tau_{01}} \begin{pmatrix} 1 & \rho_{01} \\ \rho_{01} & 1 \end{pmatrix} \begin{pmatrix} E_{f,1} \\ E_{b,1} \end{pmatrix} \qquad 3.4$$

(Maulini, 2006; Orfanidis, 2002).

As the electric field continues through the first layer of anti-reflective coating, d1, some of the light may be absorbed by the media. At the next boundary, another wave is reflected back through the coating. This is reflected in the equation for the dephasing matrix

$$\begin{pmatrix} E_{f,d_1} \\ E_{b,d_2} \end{pmatrix} = \begin{pmatrix} e^{-ik_1 d_1} & 0 \\ 0 & e^{ik_1 d_1} \end{pmatrix} \begin{pmatrix} E'_{f,d_1} \\ E'_{b,d_2} \end{pmatrix} \qquad 3.5$$

The angular wavenumber, $k_1 = \frac{n_1 2\pi}{\lambda}$, also uses the complex index of refraction (Maulini, 2006; Orfanidis, 2002).

When there is more than one interface, as in our experiment, the entire structure is described by a 2×2 matrix, S, formed by multiplying the matching matrix with the dephasing matrix. For our two layer AR coatings, the transfer matrix S is

$$S = \frac{1}{\tau_{01}}\begin{pmatrix} 1 & \rho_{01} \\ \rho_{01} & 1 \end{pmatrix} \bullet \begin{pmatrix} e^{-ik_1 d_1} & 0 \\ 0 & e^{ik_1 d_1} \end{pmatrix} \bullet \frac{1}{\tau_{12}}\begin{pmatrix} 1 & \rho_{12} \\ \rho_{12} & 1 \end{pmatrix} \bullet \begin{pmatrix} e^{-ik_2 d_2} & 0 \\ 0 & e^{ik_2 d_2} \end{pmatrix} \bullet \frac{1}{\tau_{2air}}\begin{pmatrix} 1 & \rho_{2air} \\ \rho_{2air} & 1 \end{pmatrix}$$

(Orfanidis, 2002) 3.6

Finally, reflectivity is found by

$$R = \left(\frac{|S_{21}|}{|S_{11}|} \right)^2 \qquad 3.7$$

(Maulini, 2006; Orfanidis, 2002).

For this experiment, we wrote a module using *Mathematica*® that determines the thickness of each coating that yields the minimum reflectance for every wavelength in the mid-infrared range. (See Appendix 1) We also interpolated the index of refraction for common coating materials for given wavelengths based on literature data (Palik,1997).

SIMULATION AND DESIGN OF THE AR COATING

A single AR coating will have minimal reflectance at λ/4 if the material's refractive index is $n_{AC} \cong \sqrt{n_{sub}}$. For multiple layers of AR coating that do not meet the criteria: $n_1^2 n_{sub} = n_2^2 n_{air}$, the system is more complex. We ran the module for Maulini's (2006) anti-reflection coatings, yttrium fluoride, YF_3, and zinc selenide, ZnSe, because he found them to have minimal reflectivity over a wavelength range of 3-12μm and to be transparent to light in the mid-infrared range. He also discovered that YF_3 adhered well to the laser facet and ZnSe bonded well to the YF_3.

Unfortunately we could not use YF_3 on campus because it is toxic, so we ran our simulations with aluminum oxide, Al_2O_3, and magnesium fluoride, MgF_2, which have optical properties similar to YF_3. Al_2O_3 begins to absorb light at 6 μm and MgF_2 starts to absorb light at 6.5 μm (Palik, 1997). Nevertheless, we ran the simulation for the minimal

Wavelength (μm)	Combination 1		Combination 2		Combination 3	
	ARC Thickness Al_2O_3 (nm)	ARC Thickness ZnSe (nm)	ARC Thickness MgF_3 (nm)	ARC Thickness ZnSe (nm)	ARC Thickness YF_3 (nm)	ARC Thickness ZnSe (nm)
3	308.612	54.6596	212.873	107.706	236.395	94.4407
3.5	350.054	69.256	247.326	126.438	274.502	111.089
4	386.644	86.5801	281.345	145.476	309.886	129.329
4.5	419.318	106.217	314.884	164.847	349.438	145.27
5	450.097	126.932	347.828	184.617	385.757	163.094
5.5	492.327	141.124	380.166	204.795	421.251	181.444
6	519.069	164.133	411.845	225.413	453.153	201.897
6.5	535.719	193.039	442.77	246.526	482.796	223.705
7	550.153	223.354	472.698	268.276	510.984	246.416
7.5	561.138	255.712	502.482	290.175	538.88	269.366
8	568.808	289.99	531.05	312.839	567.711	291.853
8.5	573.129	326.541	558.282	336.606	594.175	316.021
9	574.437	364.71	584.37	360.857	620.841	339.914
9.5	561.18	399.973	609.358	386.118	647.682	364.069
10	566.387	447.75	631.815	412.954	675.342	387.861
10.5	558.196	491.984	655.085	439.437	Indices of Refraction for YF_3 for $\lambda > 10$ μm was not available.	
11	545.802	538.012	675.91	467.455		
11.5	529.88	586.733	694.62	497.209		
12	510.723	634.744	711.998	527.907		

Figure 9: AR Coatings for Zero Reflectivity. Data from the simulation where thicknesses yield the minimum reflectivity for each wavelength.

reflectivity for a range between 3-12 μm (See Table 1) and noticed that both Al_2O_3-ZnSe and MgF_2–ZnSe double coatings can reach zero reflectivity for the wavelengths range, see Table 1.

Still, zero reflectivity for a single wavelength does not ensure the broadband coverage necessary for a tunable laser. The thickness of the AR coating cannot vary with wavelength therefore we need to determine the thickness for each material that has the lowest reflectivity over the largest wavelength range. We subsequently carried out multiple simulations; graphing "Reflectivity vs. Wavelength" for different thicknesses of Al_2O_3-ZnSe and MgF_2-ZnSe (See Appendix for examples), looking for thicknesses that gave us the least reflectivity over the broadest wavelength range, concentrating our efforts in the 9.5-11 μm since the QCL emits radiation in that range, see Figure 9. Once we found a suitable thickness, we compared the reflectivity of our AR coating with the YF_3-ZnSe benchmark that Maulini produced (See Graph 1). After running the computer simulations, we opted to deposit a layer of Al_2O_3 at 561nm and a 400 nm layer of ZnSe on the QCL for the experiment.

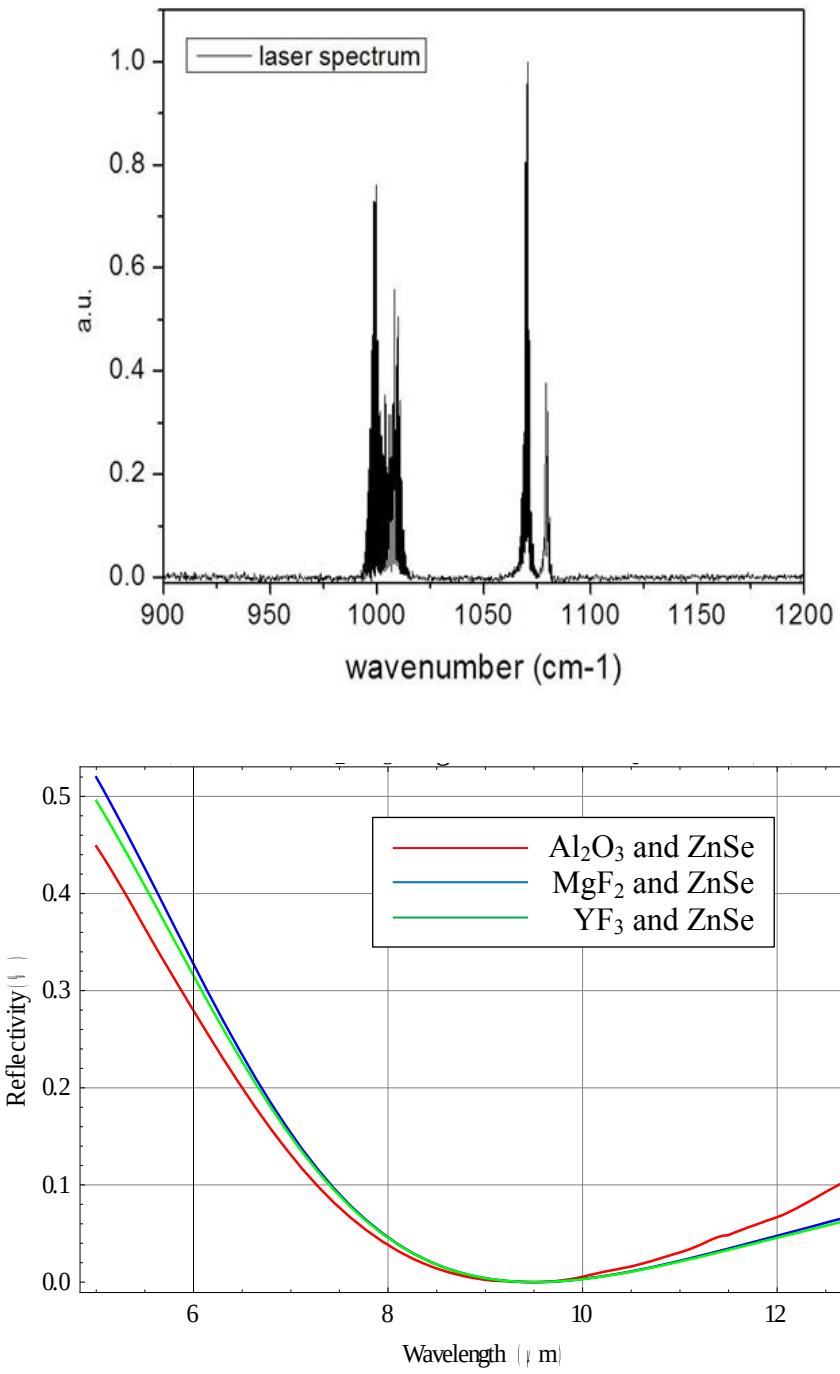

Figure 10: (Top) The QCL's spectrum where λ=1/υ. (Bottom) Comparison of the reflectivity of various AR coatings on a QCL substrate at 9.5 μm based on simulations.

DEPOSITION OF THE AR COATING-METHODS AND MATERIALS

The Al_2O_3 AR coating was deposited on three QCL's with an Electron Beam Physical Vapor Deposition system, EBPVD. Lasers were prepared by removing the wires and masking the parts that did not need to be coated. The laser was then taped on the sample holder with the front facet facing down. A piece of silicon wafer was also taped on the sample holder as a reference to calibrate the final deposited thickness. The sample holder was then attached to the manipulator shaft within the chamber. The chamber was closed and nitrogen was poured into the well for the cryogenic-pump, which is necessary for the low pressures needed for deposition. When the pressure in the chamber reached 7.5 $\times 10^{-6}$ Torr, the electron beam bombards the target material and deposition begins.

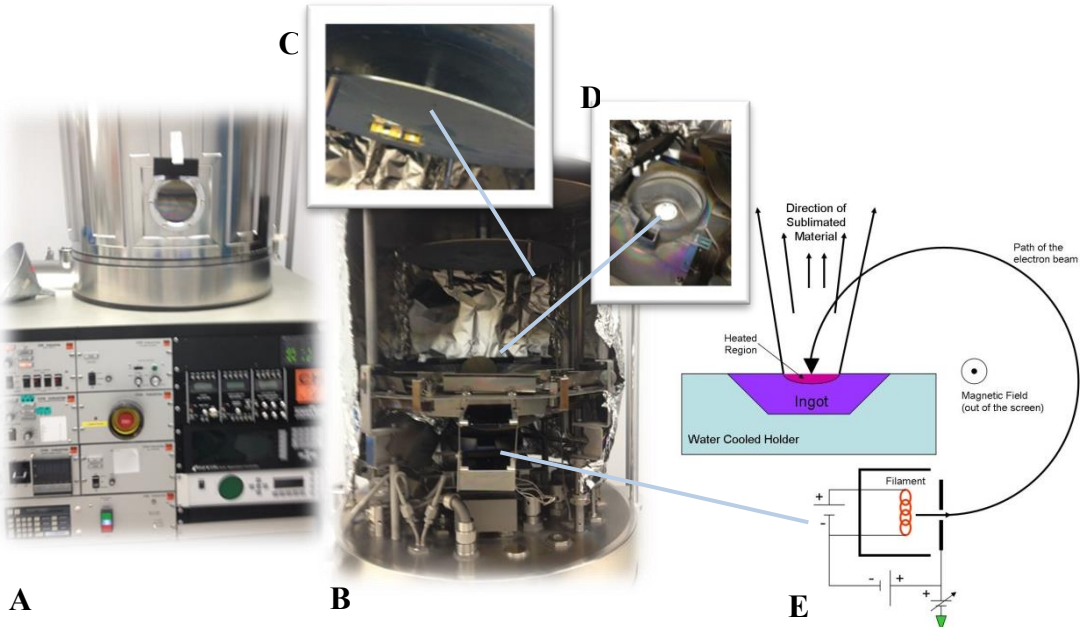

Figure 11: The EBPVD system. A) Chamber closed, with control board. B) The deposition chamber opened, the inset, C) shows the sample holder, the yellow object is the tape holding the QCL's in place. Inset D) shows the placement of the crucible with the material. E) The electron beam is shot through a magnetic field, curving the beam so it hits the crystals (Electron Beam Physical Vapor Deposition, 2006).

The accelerating voltage from the gun was 9.82 kV, and the evaporation rate was 1Å/s. The temperature in the chamber began at 40 °F but slowly rose to 100 °F. High temperatures create a different evaporation condition and change the refractive index of the evaporated material. Also, based on previous experience, high temperatures make it difficult to get a uniform coating on a small facet. Stresses caused during the heat up and cool down process crack the film. Therefore it was necessary for the EBPVD system to be turned off to allow the chamber to cool when temperatures rose above 100 °F. This allows the conditions within the chamber to remain relatively constant and ensure a uniform film thickness. The system was stopped to calibrate the deposition rate when the EBPVD system read 2.295 kÅ, measured with an internal crystal quartz.

The depth of aluminum oxide coating on a silicon wafer was verified with an ellipsometer (see Figure 11). (Ellipsometers measure the changes in reflected light from

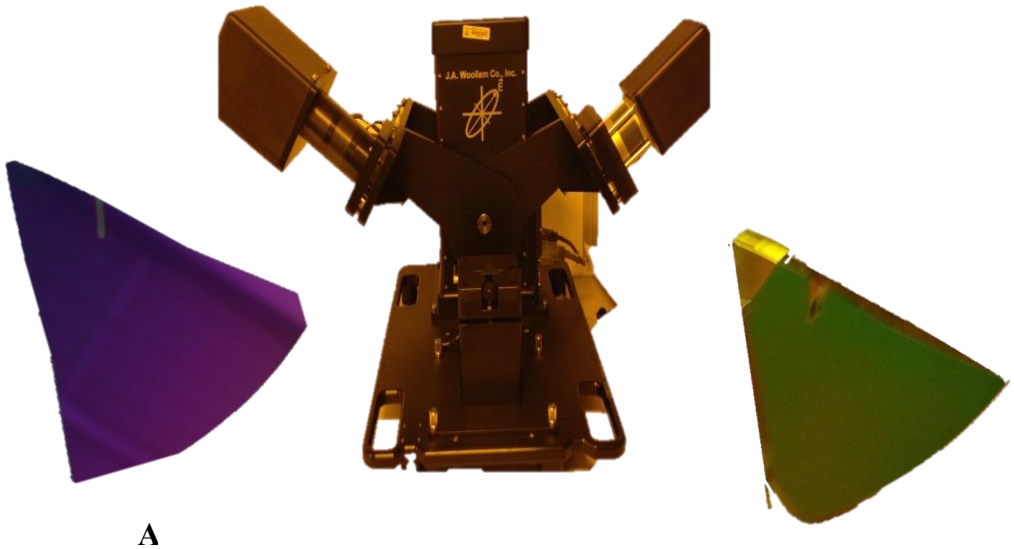

Figure 12: The Ellipsometer. A. Silicon wafer piece with Al2O3 coating. B) The ellipsometer measures the thickness of thin film accurately by measuring the changes in amplitude and phase of the incident radiation. C) The piece of silicon wafer with ZnSe coating.

the incident radiation. Accurate measurements can be made for films less than a hundred nanometers to a few microns thick (Woollam, Co.,Inc.).) The measured thickness for the first coat of aluminum oxide on the piece of silicon wafer was 435 nm. Not having reached our target of 561nm, it was necessary to put the lasers back into the EBPVD system. The second session in the chamber brought the thickness of Al_2O_3 to 572 nm. In order to have zero reflectance at 8.5 μm wavelengths, we would need to apply a 327 nm thick layer of zinc selenide (see Figure 9).

The ZnSe was applied with a sputtering deposition system, another physical vapor deposition method for making thin films. The lasers were prepared for the sputtering system by placing them in specially milled openings in the stage (Figure 13) that exposed

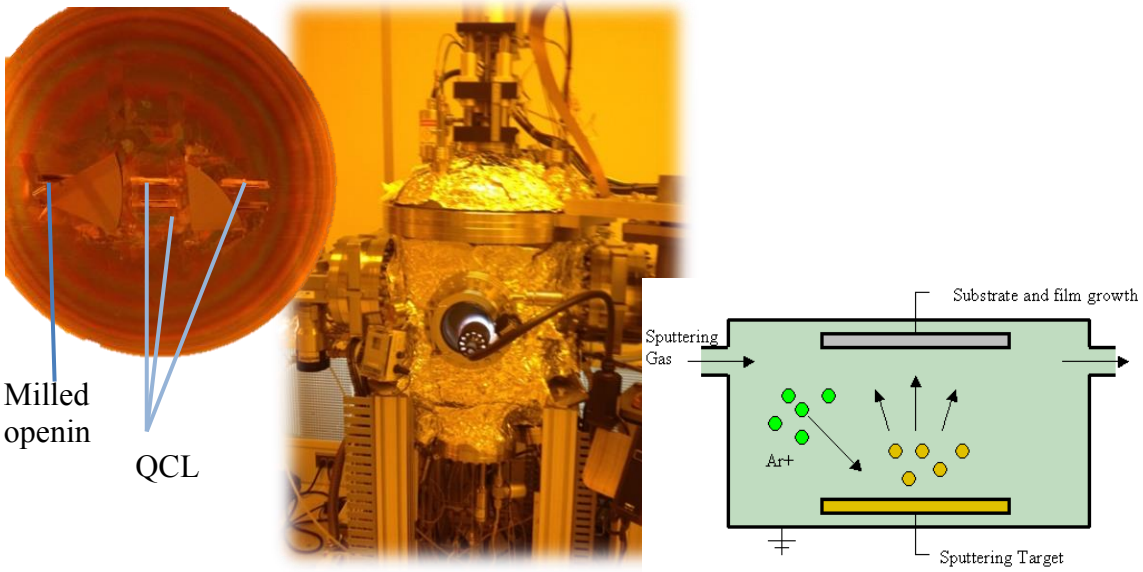

Figure 13: The sputter deposition system. A) The exposed surface of the QCL on the custom milled stage with silicon wafers. B) The Sputtering Deposition system. C) Model of the Sputtering Deposition system. A stream of high energy particles, usually argon plasma, hits a target material. The atoms on the surface of the material are knocked free from its crystal. The sputter, ejected atoms from the target material, diffuse throughout the chamber and coat the substrate (Sputter deposition, 2007).

their front facets. Just like the aluminum oxide deposition, pieces of the silicon wafer were also placed on the stage, close to the laser facet as a reference to calibrate film thickness. The stage was placed in the load lock to allow the loading area to reach the same pressure as the chamber. When the valve opened, the stage was moved into the chamber, onto the rotating assembly. The manufacturer's software controlled the sputtering system, maintaining the pressure at 15.0 mTorr, with 100 W of power. The final thickness of the ZnSe film was verified with the ellipsometer on the silicon wafer. We achieved a thickness of 392 nm, which is close to the thicknesses needed to have zero reflectivity at 9.5 μm (see Figure 9).

TESTING LASER REFLECTIVITY

Before the AR coating was deposited on the lasers, light-current and voltage-current characteristics were recorded with LabVIEW software. The picture below shows the experimental apparatus. The QCL was mounted to an 'L' bracket copper block and connected to the pulse generator. Channels 1and 2 of the oscilloscope measured laser

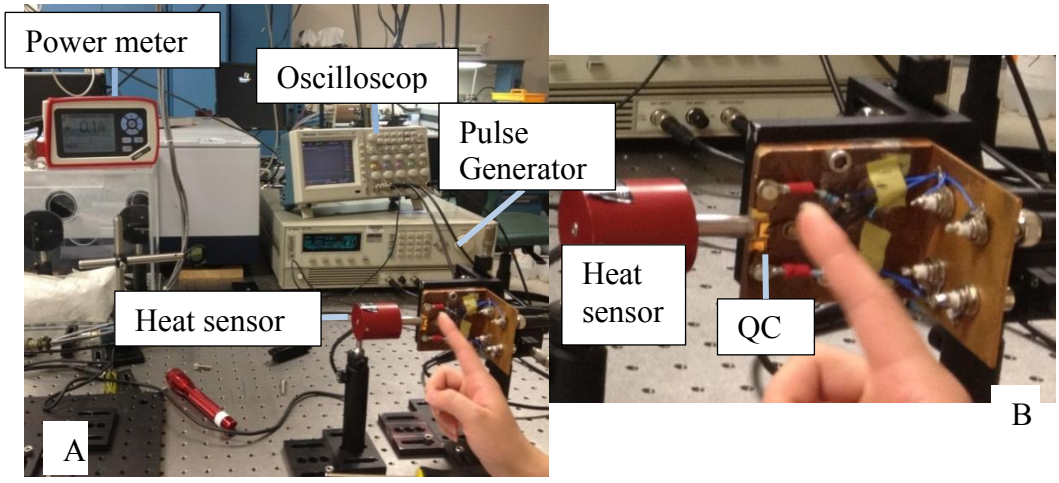

Figure 14 : A)The experimental setup. B) Close-up of the mounted QCL, with heat sensor on laser output.

current and voltage, respectively. A power meter was used to measure the radiation from the laser facet (See Figure 14). A cardboard box was placed over the laser and heat sensor, to prevent the sensor from measuring heat from other sources. The LabVIEW program recorded the light-current characteristic by controlling the pulse generator that increased the current going through the QCL gradually while measuring the generated radiation in the power meter. The wires were soldered back on the AR coated QCL's before the experiment was repeated.

Chapter 4: Results and Conclusion

RESULTS

The cleaved surfaces of the QCL have an initial reflectivity of 30% providing the mirrors for the resonance cavity. Adding the AR coating to front facet essentially "breaks" that mirror and increases the mirror loss for the QCL, Therefore, we expected an increase in threshold current. Figure 15 shows the effects of a double layer AR coating on a 1.64 mm QCL emitting radiation at approximately 9.5 μm. Our results show a 0.47 increase in threshold current after the coating, or increasing by a factor ρ=1.27. The actual reflectivity of our device with a waveguide loss of α_ω= 8 cm^{-1} (Maulini, 2006) is calculated by:

$$R_{AC} = R_0^{2\rho-1} e^{-2L(\rho-1)\alpha_\omega} \cong 0.077 \qquad 4.1$$

where R_0 is the initial reflectivity of the laser. The addition of the AR coating decreased the reflectivity from 30% to 7.7%.

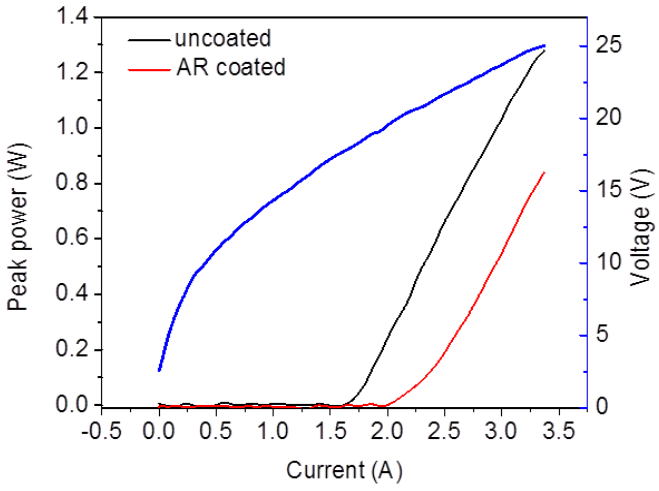

Figure 15: The before and after AR coating comparison of the threshold current of a Fabry-Perot laser ridge. Blue curve shows the optical power vs. the current with the coated facet. The black curve, the uncoated facet; and the red curve, the AR coated one.

Discussion

The reflectivity of our AR coating was higher than anticipated. This may be due to the nature of the aluminum oxide coating. Under very high heat, such as the heat experienced by the EBPVD chamber, Al_2O_3 can dissociate into AlO_3 and Al_2O ions which may have optical properties that are different from the original crystal (Electron beam physical vapor deposition, 2006). One method to determine this would be to deposit a very thick film and check the refractive index in the Mid-IR range with Fourier transform infrared (FTIR) spectroscopy. Another way to measure the actual index of refraction is to use a Mid-IR ellipsometer, which is not available in the MRC cleanroom. Unfortunately, we did not have time to investigate this aspect of aluminum oxide. It took six hours to deposit 572 nm using the EBPVD system, so it would possibly take 24 hours to deposit a few microns with continuous monitoring. The high reflectivity results of the AR coating may also relate to the ZnSe sputtering. The refractive index from EBPVD method and sputtering method differs from accepted values based on ellipsometer measurements in visible range.

CONCLUSION

A double layer AR coating with a different material combination was investigated. The theoretical model involving the reflection and transmission of multiple layers was built based on the propagation matrix method. Guided by our simulation, a combination of 561 nm of Al_2O_3 and 400 nm of ZnSe was able to give zero percent reflectivity at 9.5 μm wavelengths. The experiment was done by coating the laser with Al_2O_3 using an electron-beam evaporator and depositing ZnSe with a sputtering system. A 392 nm ZnSe layer over a 572 nm Al_2O_3 layer was achieved, producing 7% reflectivity for the QCL facet.

Chapter 5: The Research Experience

The scope of this research project is well beyond the limitations of high school physics. I doubt there is a high school in America with access to a clean room or the benefit of the extra time needed to deposit thin film on a substrate. However, there are several ways students can benefit from the engineering experience.

SIMULATIONS

I used Mathematica to simulate AR coating thicknesses before going into the cleanroom. It proved to be a cost saving tool since evaporating film on a substrate takes hours, whereas the simulation only takes seconds. One way adapt the engineering experience to the classroom is to have the students do a simulation before they begin a lab. Time constraints prevent us from writing our own programs, however, they could use Excel or their calculator to graph simple relationships or use PhET™, open source simulations, to preview a lab. Both methods would aid students in their predictions, build background, and help them become better acquainted with the concepts. The PhET simulations allow the students to "play" with a concept, such as electric fields, before going in the lab to make and measure one. The simulations are especially useful if the investigation involves an engineering challenge. For example, after students perform the "Masses and Springs" PhET simulation at the computer lab, it is followed with the "Barbie Bungee" challenge in the physics lab.

THE CLEAN ROOM

Going into the cleanroom and learning about the equipment used in nanotechnology was by far the most exciting part of my research experience. It was a revelation to see the concepts I teach being applied in so much technology. Since I

cannot take them into the clean room, I will introduce my students the technology in another way. A common test question in AP Physics for quantum mechanics involves calculating the photon energy emitted when an electron falls back to ground state. I could teach this concept using QCL's, explaining how they are engineered. Including QCL in the stem will add relevance to the problem. Clean room technology is also relevant when we discuss electromagnetism. A classic AP question involves finding the radius of the circular path of a proton shot through a magnetic field. My students want to know why a random proton is being shot through a magnetic field. Now I can show them the technology on which this problem is based. Of course, I can always apply the technology to Newtonian mechanics. Asking about the momentum of an Al^{+} ion in an EB chamber requires them to change the scale of their thinking. The technology is not new and the textbook describes these applications, but the students do not put the two together until they can visualize the process. I can now provide a story making this technology relevant.

Chapter 6-Application to Practice-The MASEE Program

DEVELOPING ENGINEERING AWARENESS

As a physics teacher, I do not often have the opportunity to teach specific career paths in engineering. I try to make my students aware of the various careers in physics through class projects. The first project I give is a book cover project. Students research different careers where knowledge of physics is necessary. Many of the book covers involve engineering, however, most focused on civil or mechanical engineering. Like my students, I did not fully appreciate the scope and breadth of engineering until the first MASEE lesson on "Engineering Achievements of the 20th Century." Even so, it was not until I began doing research for this project that I realized how much I focused on mechanical and civil engineering in class, rather than broadening the world of engineering for my students.

Luckily, changing my practices can easily be done with a little foresight and planning. Each time I introduce a unit, it will include "Engineering Achievements" specific for that unit. For instance, when we begin discussing energy conservation, we could discuss how automobiles use advanced materials to reduce weight, improving fuel efficiency without sacrificing safety. Now, when I begin the "Light" unit, I will tell the story of lasers, or later, when we start "Quantum Physics," I can engage them with nano-technology and how a QCL exploits the quantum world to produce coherent light. The added advantage is that all the engineering achievements use more than one physics concept, so spiraling back to a previous topic or previewing a future one will be easy.

In addition to engagement activities, adding a "research engineering" component to each project would provide students with specific information about pursuing a career in engineering. The next time we do the trebuchet project, students can research engineers that specifically use the concept of projectile motion in their designs. This

allows students to be creative. Many will still report on mechanical engineers, but a few may include aerospace engineering. Moving beyond general engineering fields into the more specialized areas will help students appreciate just how much engineering has infiltrated and improved their lives.

DEVELOPING ENGINEERING HABITS OF MIND

One of the newest trends in education is the "Professional Learning Communities," PLC, where teachers meet to discuss common concerns. My district has embraced this idea and PLC meetings have been a part of the planning process for the last three years. I have been the only physics teacher at my school until last year when the "4x4" required all students to take physics and the physics EOC (10^{th} grade only). The influx of new students brought in two new teachers. No longer alone, the PLC expected me to lead the lesson planning. One thing I picked up from the MASEE program is that lesson planning is indeed a design process, requiring the same habits of mind necessary for engineering where communication and collaboration are most important.

I have never been one to design a lesson completely on my own. I gather ideas from a multitude of sources and choose those that are most feasible, i.e. we have the needed equipment; or can be done within the time constraints. With two new teachers this year, I had to implement true collaboration. Incorporating their ideas into my lessons was painless; on the other hand, sharing ideas with the team was a little uncomfortable. I had to learn to present my ideas and back them with reasons or research. Our priority became what is best for the students rather than what is best for us. Whether it we choose a new activity, such as using graphic organizers, or adopted a new approach, like Problem Based Learning (PBL), we were mindful of student's learning. Unfortunately,

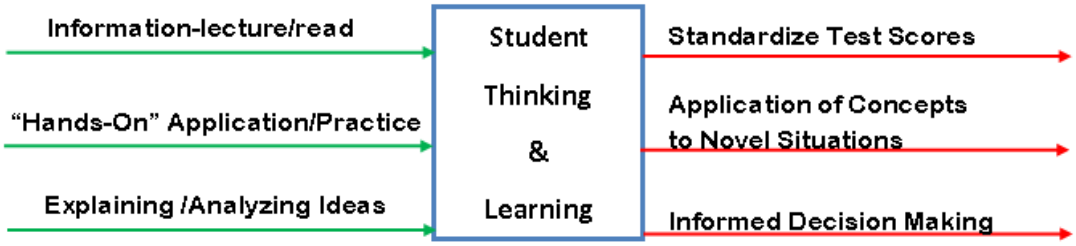

Figure 16: Students as black box. Engineering habits of mind help students make better decision as well as better problem solvers.

the collaboration that occurred between physics teachers about student learning occurred in my classroom during planning period.

Unfortunately, the added pressure from the EOC test meant last year's PLC meetings focused on outputs rather than inputs, see Figure 16. Test scores are just one outcome of a well-rounded education. This year, I hope to shift the attention from outcomes to teaching methods and include other forms of assessments including projects. Engineering projects or challenges reinforce the "Engineering Habits of Mind" that we expect from a 21st century student. Engineering challenges require students to collaborate with each other, to analyze a system and to be creative problem solvers, skills they will need in the future even if they choose a different career path.

I plan on incorporating more models in the future. In the past I only emphasized mathematical modeling. I thought physical models too juvenile, something best reserved for freshman biology to keep them busy. However, in the MASEE program, we used a variety of models to analyze and investigate system interactions. We used physical models, toys, to investigate rotational motion. We used diagrams to investigate the causes and effects in a system. Last year my students expressed trouble with knowing which equation to use to solve a word problem. This occurs every year with the first unit,

kinematics, because the students see four very similar equations, with similar variables, but fail to distinguish the differences between them. Together, we made a flow chart on how to solve a word problem. This metacognition technique worked much better than simply telling them to use the GUESS (Given, Unknown, Equation, Substitution and Solution) method because it reminded them to look at what information was left out of the problem.

DEVELOPING AN UNDERSTANDING OF THE DESIGN PROCESS

The research experience gave me the chance to immerse myself in the engineering world. My initial research addressed the "Project Description" part of the design process. Through research, I began to understand why AR coatings are used on lasers along with some of the design constraints, e.g. ability to stick to the laser. The simulation allowed for multiple runs of various transparent materials, although not all the materials were available. I could use the same program with different substances and the simulation would let me know how thick the coating would need to be. Although it was frustrating at times, I understood the value of it, especially when fabricating the AR coating can take over five hours. Fabricating and testing the AR coat introduced me to technology that I had previously only read about. In science, experiments test relationships among the variables. In engineering, the experiments are testing for improvements from a previous design. Time did not permit multiple iterations with different thicknesses and we did not have the resources to try other materials.

DEVELOPING KNOWLEDGE FOR AND OF ENGINEERING TEACHING

I entered the MASEE program because I wanted to make my students better problem solvers. The learned that if I want to help them solve problems, I need to give them problems they can solve creatively. There should be more than one way to

tackle the problem and more than one correct answer. Scaffolding may be necessary in the beginning, but that is how learning occurs. To that end, this year, instead of introducing the lesson's objective, I introduced a problem, usually accompanied with a demonstration so they can visualize it as well. Last year, instead of the usual momentum demonstration, I began by asking the students if it were possible for a moving object to hit a stationary object and come to rest. Then I asked what conditions are necessary for both objects to come to rest after the collision. The students were more engaged in the lesson and it felt more like "Just-in-Time" learning than a lecture. Also, students that already know one solution, benefit from learning alternate solutions.

There is also something intrinsically motivating about a challenge. Many of the "verification" labs can easily be changed into a design challenge and I am in the process of changing them. My students enjoyed the challenge of building a bumper that had the smallest force when it hit the "wall." Even when a challenge is not given, students often challenge themselves. Every year, they see who could get the most standing waves on the string during the lab. Teaching sophisticated ideas, like torque, using toys is another idea to increase student engagement. Toys are an excellent "hook" because they are disarming and fun. In the MASEE program, we used toys to build a word wall. It also served as background for circular motion and torque.

Next school year, I will be teaching Project Lead the Way's, Engineering Design and Development, EDD. The class centers on the design process from start to finish and with at least one iteration on the project. Having experienced "real-world" engineering through the research project, I feel uniquely qualified to teach the class. I can incorporate all of the MASEE program's structured lessons to teach the design process. I now have lessons to help students boost their creativity or determine the needs of a product. Not

only will these lessons engage them in the design process, they will have a more professional product and presentation in the end.

Appendix A

INTERPOLATION OF REFRACTIVE INDICES OF SEVERAL CRYSTALS

```
al2o3={{1.550,1.742},{2.480,1.726},{2.703,1.719},{2.857,1.714},{3.030,1.709},{3.571
,1.692},{3.846,1.681},{4.00,1.674},{4.545,1.647},{4.762,1.636},{5.000,1.624},{5.556,
1.624},{6.250,1.571},{6.667,1.534},{7.143,1.485},{7.692,1.419},{8.333,1.325},{9.091,
1.181},{10.00,0.925},{10.20,0.847},{10.53,0.693},{10.75,0.550},{10.99,0.340},{11.11,
0.213},{11.49,0.101},{12.05,0.116},{12.50,0.083},{12.99,0.090},{13.51,0.104},{14.09,
0.131},{14.49,0.165},{15.15,0.317},{15.63,1.222},{16.13,0.852}};
indexAl2O3=Interpolation[al2o3];

alphaal2o3={{2.00,0},{3.00,0},{4.00,0},{5.00,0},{5.556,0.002},{6.667,0.004},{7.143,0.
005},{7.692,0.007},{8.333,0.011},{9.091,0.017},{10.00,0.034},{10.20,0.003},{10.53,0.
058},{10.75,0.081},{10.99,0.147},{11.11,0.249},{11.49,0.634},{12.05,1.017},{12.50,1.
287},{12.99,1.571},{13.51,1.890},{14.09,2.278},{14.49,2.607},{15.15,3.350},{15.63,4.
181},{16.13,3.306}};
niAl2O3=Interpolation[alphaal2o3];

yf3={{0.404656,1.52788},{0.4471,1.52385},{0.5015,1.52025},{0.546074,1.51818},{0.5
76959,1.51690},{0.587561,1.51657},{0.667815,1.51421},{0.706519,1.51341},{1.01398
,1.50944},{1.08297,1.50885},{1.12866,1.50843},{1.3622,1.50689},{1.52952,1.50597},
{1.6066,1.50530},{1.6932,1.50496},{1.81307,1.50309},{2.1526,1.50236},{2.4374,1.50
065},{3.2389 ,1.49446},{3.3036,1.49395},{3.4115,1.49293},{3.4199,1.49274},
{3.5524,1.49149},{3.7077,1.48999},{3.7601,1.48953},{3.8480,1.48877},{3.9788,1.478
14},{4.258,1.48416},{4.3769,1.48262},{4.5960,1.48001},{4.6885,1.47873},{4.8598,1.4
7639},{5.1088,1.47263},{5.3036,1.46981},{6.00,1.45},{8,1.37},{10,1.30}};
indexYF3=Interpolation[yf3] ;

mgf2={{2,1.3678},{2.5,1.3643},{3.0303,1.3597},{3.571,1.354},{4.000,1.3488},{4.5455
,1.3413},{5.00,1.334},{5.5556,1.324},{6.0606,1.3138},{6.6667,1.2998},{7.1429,1.287}
,{7.4074,1.281},{8.00,1.264},{8.6957,1.240},{9.0909,1.224},{9.5238,1.206},{10.0000,
1.18},{10.638,1.15},{11.111,1.12},{12.195,1.04},{13.158,0.95},{14.286,0.79},{15.152,
0.61},{16.129,0.28},{17.241,0.14},{18.519,0.14},{20.000,0.17}};
indexMgF2=Interpolation[mgf2];

znse={{3.000,2.437},{3.500,2.435},{4.000,2.433},{4.500,2.431},{5.000,2.429},{5.500,
2.427},{6.000,2.425},{6.500,2.423},{7.000,2.421},{7.500,2.419},{8.000,2.417},{8.500,
2.414},{9.000,2.412},{9.500,2.409},{10.00,2.406},{10.50,2.403},{11.00,2.400},{11.50,
2.396},{12.00,2.392},{12.50,2.389},{13.00,2.384},{13.50,2.380},{14.00,2.376},{14.5,2
.371},{15.00,2.366}{15.5,2.361},{16.00,2.355}};
indexZnSe=Interpolation[znse];
```

Appendix B

THICKNESSES MODULE FOR ZNSE AND YF3

```
R3[λ_,d1_,d2_]:= Module[{nsub,n1,n2,nAir,karc1,karc2,matS},
    nsub=3.2;nAir=1;n2=indexZnSe[λ];n1=indexYF3[λ];
                karc1=n1*2π/(λ*10^-6);karc2=n2*2π/(λ*10^-6);
    matS=Dot[(_{{(n1+nsub)/(2 nsub), (-n1+nsub)/(2 nsub)},{(-n1+nsub)
                /(2 nsub), (n1+nsub)/(2 nsub)}}_),(_{{ⅇ-ⅈ d1*(10^-9)
                karc1, 0}, {0, ⅇ^ⅈ d1 *(10^-9)karc1}}_),_(_{{(n1+n2)/(2 n1),
                 (n1-n2)/(2 n1)},{(n1-n2)/(2 n1), (n1+n2)/(2 n1)}}_),
                (_{{ⅇ-ⅈ d2*(10^-9) karc2, 0}, {0, ⅇ^ⅈ d2 *(10^-9)karc2}}_),
                (_{{(n2+nAir)/(2 n2), (n2-nAir)/(2 n2)},{(n2-nAir)/(2 n2),
                (n2+nAir)/(2n2)}}_)];(Abs[matS[[2,1]]])^2/(Abs[matS[[1,1]]])^2];

Table[{λ,Minimize[R3[λ,d1,d2],{d1,d2}]},{λ,3,10,0.5}]

        {{3.,{8.89509×10^-17,{d1→236.395,d2→94.4407}}},

        {3.5,{2.1548×10^-17,{d1→274.502,d2→111.089}}},

        {4.,{8.144×10^-19,{d1→309.886,d2→129.329}}},

        {4.5,{2.10916×10^-17,{d1→349.438,d2→145.27}}},

        {5.,{2.08361×10^-17,{d1→385.757,d2→163.094}}},

        {5.5,{1.81996×10^-17,{d1→421.251,d2→181.444}}},

        {6.,{3.78359×10^-22,{d1→453.153,d2→201.897}}},

        {6.5,{6.12746×10^-18,{d1→482.796,d2→223.705}}},

        {7.,{1.97872×10^-17,{d1→510.984,d2→246.416}}},

        {7.5,{1.97388×10^-17,{d1→538.88,d2→269.366}}},

        {8.,{5.42979×10^-19,{d1→567.711,d2→291.853}}},

        {8.5,{1.95252×10^-17,{d1→594.175,d2→316.021}}},

        {9.,{1.01908×10^-18,{d1→620.841,d2→339.914}}},

        {9.5,{1.6207×10^-17,{d1→647.682,d2→364.069}}},

        {10.,{2.03449×10^-17,{d1→675.342,d2→387.861}}}}
```

THICKNESSES MODULE FOR ZNSE AND MGF2

```
R4[λ_,d1_,d2_]:=
  Module[{nsub,n1,n2,nAir,karc1,karc2,matS},
        nsub=3.2;nAir=1;n2=indexZnSe[λ]; n1=indexMgF2[λ]+I*4.4 10^-4;
          karc1=n1*2π/(λ*10^-6);karc2=n2*2π/(λ*10^-6);
        matS=Dot[(_{{(n1+nsub)/(2 nsub), (nsub-n1)/(2 nsub)},
        {(nsub-n1)/(2 nsub), (n1+nsub)/(2 nsub)}}_),
        (_{{ⅇ-ⅈ *d1 *10^-9* karc1, 0},{0, ⅇ^ⅈ *d1*10^-9* karc1}}_),
        (_{{(n1+n2)/(2 n1), (n1-n2)/(2 n1)},{(n1-n2)/(2 n1), (n1+n2)/(2 n1)}}_),
        (_{{ⅇ-ⅈ *d2*10^-9* karc2, 0},{0, ⅇ^ⅈ *d2*10^-9* karc2}}_),
        (_{{(n2+nAir)/(2 n2), (n2-nAir)/(2 n2)},{(n2-nAir)/(2 n2),
        (n2+nAir)/(2 n2)}}_)];
        (Abs[matS[[2,1]]])^2/(Abs[matS[[1,1]]])^2];

Table[{λ,Minimize[R4[λ,d1,d2],{d1,d2}]},{λ,3,12,0.5}]
```

{{3.,{1.99718×10^-17,{d1→212.873,d2→107.706}}},
{3.5,{1.72688×10^-17,{d1→247.326,d2→126.438}}},
{4.,{2.30264×10^-19,{d1→281.345,d2→145.476}}},
{4.5,{1.20743×10^-17,{d1→314.884,d2→164.847}}},
{5.,{2.00918×10^-17,{d1→347.828,d2→184.617}}},
{5.5,{2.06729×10^-19,{d1→380.166,d2→204.795}}},
{6.,{3.74889×10^-18,{d1→411.845,d2→225.413}}},
{6.5,{2.04138×10^-17,{d1→442.77,d2→246.526}}},
{7.,{1.57153×10^-18,{d1→472.698,d2→268.276}}},
{7.5,{5.39178×10^-19,{d1→502.482,d2→290.175}}},
{8.,{2.08172×10^-17,{d1→531.05,d2→312.839}}},
{8.5,{2.10592×10^-17,{d1→558.282,d2→336.606}}},
{9.,{1.42979×10^-17,{d1→584.37,d2→360.857}}},
{9.5,{3.71854×10^-20,{d1→609.358,d2→386.118}}},
{10.,{2.20717×10^-17,{d1→631.815,d2→412.954}}},
{10.5,{2.33377×10^-17,{d1→655.085,d2→439.437}}},
{11.,{1.02281×10^-17,{d1→675.91,d2→467.455}}},
{11.5,{2.3276×10^-17,{d1→694.62,d2→497.209}}},
{12.,{2.38462×10^-17,{d1→711.998,d2→527.907}}}}

THICKNESSES MODULE FOR ZNSE AND AL2O3

```
R1[λ_,d1_,d2_]:=
    Module[{nsub,n1,n2,nAir,karc1,karc2,matS},
      nsub=3.2;nAir=1;n2=indexZnSe[λ];n1=indexAl2O3[λ]+I*niAl2O3[λ];
      karc1=n1*2π/(λ*10^-6);karc2=n2*2π/(λ*10^-6);
      matS=((n1+nsub)/(2 nsub))*((n1+n2)/(2 n1))*((n2+nAir)/(2 n2))*
      (Dot[(_{{1, (-n1+nsub)/(n1+nsub)},{(-n1+nsub)/(n1+nsub), 1}}_),
      (_{{ⅇ-ⅈ (d1*10^-9) karc1, 0},{0, ⅇ^ⅈ (d1*10^-9) karc1}}_),
      _(_{{1, (n1-n2)/(n1+n2)},{(n1-n2)/(n1+n2), 1}}_)_,
      (_{{ⅇ-ⅈ (d2*10^-9) karc2, 0},{0, ⅇ^ⅈ (d2*10^-9) karc2}}_),
      (_{{1, (n2-nAir)/(n2+nAir)},{(n2-nAir)/(n2+nAir), 1}}_)]);
      (Abs[matS[[2,1]]])^2/(Abs[matS[[1,1]]])^2];

      Table[{λ,Minimize[R1[λ,Al2O3,ZnSe],{Al2O3,ZnSe}]},{λ,3,12,0.5}]
      {{3.,{2.59162×10^-20,{Al2O3→308.612,ZnSe→54.6596}}},
      {3.5,{1.12862×10^-16,{Al2O3→350.054,ZnSe→69.256}}},
      {4.,{7.16376×10^-17,{Al2O3→386.644,ZnSe→86.5801}}},
      {4.5,{5.72936×10^-17,{Al2O3→419.318,ZnSe→106.217}}},
      {5.,{4.32293×10^-17,{Al2O3→450.097,ZnSe→126.932}}},
      {5.5,{7.97027×10^-17,{Al2O3→492.327,ZnSe→141.124}}},
      {6.,{8.64559×10^-18,{Al2O3→519.069,ZnSe→164.133}}},
      {6.5,{2.40827×10^-17,{Al2O3→535.719,ZnSe→193.039}}},
      {7.,{2.16513×10^-17,{Al2O3→550.153,ZnSe→223.354}}},
      {7.5,{1.99413×10^-17,{Al2O3→561.138,ZnSe→255.712}}},
      {8.,{1.26254×10^-20,{Al2O3→568.808,ZnSe→289.99}}},
```

{8.5,{1.39518×10^{-17},{Al2O3→573.129,ZnSe→326.541}}},

{9.,{2.14149×10^{-17},{Al2O3→574.437,ZnSe→364.71}}},

{9.5,{2.11765×10^{-17},{Al2O3→561.18,ZnSe→399.973}}},

{10.,{3.07613×10^{-19},{Al2O3→566.387,ZnSe→447.75}}},

{10.5,{2.69215×10^{-17},{Al2O3→558.196,ZnSe→491.984}}},

{11.,{7.55021×10^{-20},{Al2O3→545.802,ZnSe→538.012}}},

{11.5,{3.11001×10^{-17},{Al2O3→529.88,ZnSe→586.733}}},

{12.,{6.84181×10^{-17},{Al2O3→510.723,ZnSe→634.744}}}}

REFLECTIVITY GRAPHS

```
A=Plot[R1[λ,561, 400], {λ,5,13},
    PlotLabel→{"Reflectivity of 566nm Al2O3 and 447nm ZnSe on QCL at
        10μm"},PlotStyle→{Red}];
    Show[A,Frame→True,FrameLabel→{"wavelength(μm)","Reflectivity(%)"}] ;
    Show[%,GridLines→Automatic]
```

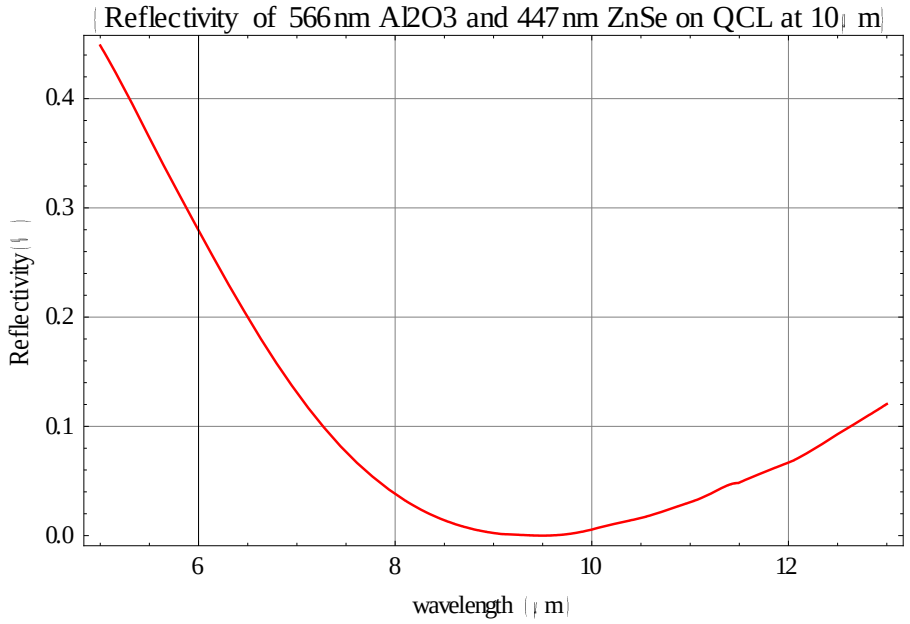

B=Plot[{R1[λ,561,400],R3[λ,675.3,387.8]},{λ,5,13},PlotLabel→{"Target vs. Actual Thickness}, PlotStyle→{Red, Blue}];

Show[B,Frame→True,FrameLabel→{"Wavelength(μm)","Reflectivity(%)"}] ;

Show[%,GridLines→Automatic]

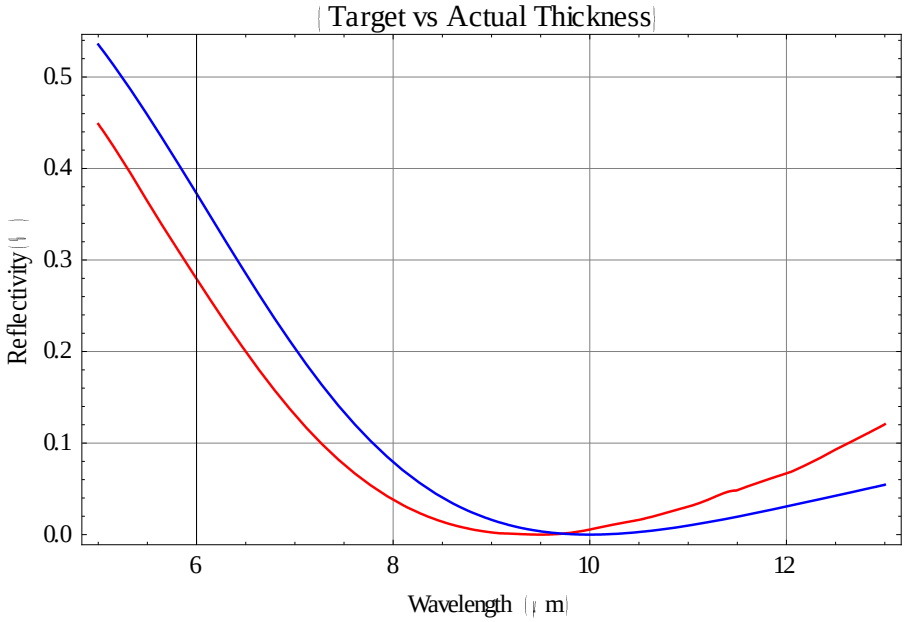

EXPERIMENT

```
R1[λ_,d1_,d2_]:=
    Module[{nsub,n1,n2,nAir,karc1,karc2,matS},
    nsub=3.2;nAir=1;n2=indexZnSe[λ];n1=indexAl2O3[λ]+I*niAl2O3[λ];
      karc1=n1*2π/(λ*10^-6);karc2=n2*2π/(λ*10^-6);
    matS=((n1+nsub)/(2 nsub))*((n1+n2)/(2 n1))*((n2+nAir)/(2 n2))*
        (Dot[(_{{1, (-n1+nsub)/(n1+nsub)},{(-n1+nsub)/(n1+nsub), 1}}_),
        (_{{ⅇ-ⅈ (d1*10^-9) karc1, 0},{0, ⅇ^ⅈ (d1*10^-9) karc1}}_),
        _(_{{1, (n1-n2)/(n1+n2)},{(n1-n2)/(n1+n2), 1}}_)_,
        (_{{ⅇ-ⅈ (d2*10^-9) karc2, 0},{0, ⅇ^ⅈ (d2*10^-9) karc2}}_),
        (_{{1, (n2-nAir)/(n2+nAir)},{(n2-nAir)/(n2+nAir), 1}}_)]);
        (Abs[matS[[2,1]]])^2/(Abs[matS[[1,1]]])^2];

Table[{λ,Minimize[R1[λ,Al2O3,ZnSe],{Al2O3,ZnSe}]},{λ,3,12,0.5}]
        {{3.,{2.59162×10^-20,{Al2O3→308.612,ZnSe→54.6596}}},
        {3.5,{1.12862×10^-16,{Al2O3→350.054,ZnSe→69.256}}},
        {4.,{7.16376×10^-17,{Al2O3→386.644,ZnSe→86.5801}}},
        {4.5,{5.72936×10^-17,{Al2O3→419.318,ZnSe→106.217}}},
        {5.,{4.32293×10^-17,{Al2O3→450.097,ZnSe→126.932}}},
        {5.5,{7.97027×10^-17,{Al2O3→492.327,ZnSe→141.124}}},
        {6.,{8.64559×10^-18,{Al2O3→519.069,ZnSe→164.133}}},
        {6.5,{2.40827×10^-17,{Al2O3→535.719,ZnSe→193.039}}},
        {7.,{2.16513×10^-17,{Al2O3→550.153,ZnSe→223.354}}},
        {7.5,{1.99413×10^-17,{Al2O3→561.138,ZnSe→255.712}}},
        {8.,{1.26254×10^-20,{Al2O3→568.808,ZnSe→289.99}}},
```

{8.5,{1.39518×10^{-17},{Al2O3→573.129,ZnSe→326.541}}},

{9.,{2.14149×10^{-17},{Al2O3→574.437,ZnSe→364.71}}},

{9.5,{2.11765×10^{-17},{Al2O3→561.18,ZnSe→399.973}}},

{10.,{3.07613×10^{-19},{Al2O3→566.387,ZnSe→447.75}}},

{10.5,{2.69215×10^{-17},{Al2O3→558.196,ZnSe→491.984}}},

{11.,{7.55021×10^{-20},{Al2O3→545.802,ZnSe→538.012}}},

{11.5,{3.11001×10^{-17},{Al2O3→529.88,ZnSe→586.733}}},

{12.,{6.84181×10^{-17},{Al2O3→510.723,ZnSe→634.744}}}}

A=Plot[R1[λ,572,392], {λ,5,13},

PlotLabel→{"Reflectivity of 572nm Al2O3 and 392nm ZnSe on QCL at 10μm"},

PlotStyle→{Red}];

Show[A,Frame→True,FrameLabel→{"wavelength(μm)","Reflectivity(%)"}] ;

Show[%,GridLines→Automatic]

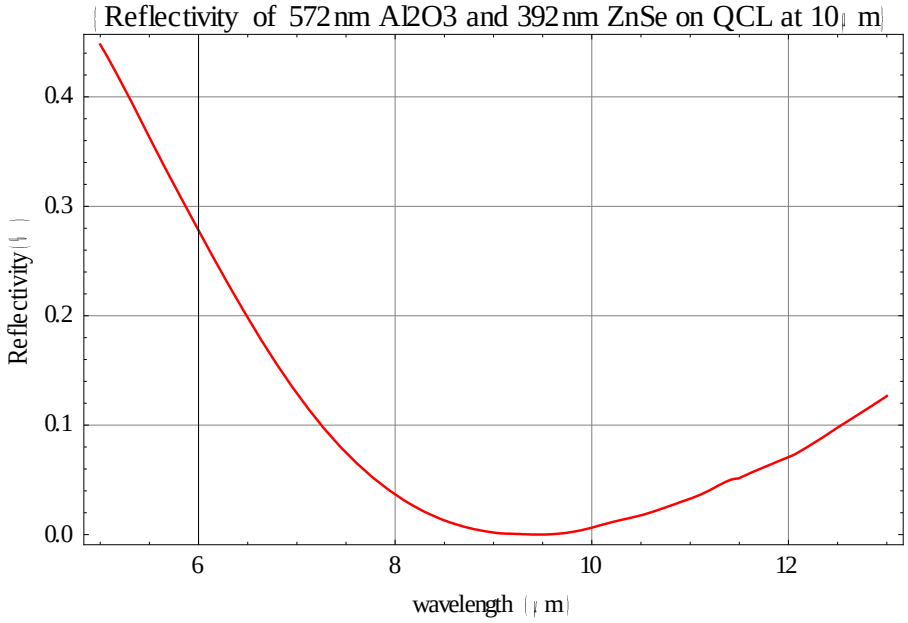

B=Plot[{R1[λ,572,392],R1[λ,561,392]}, {λ,5,13},

PlotLabel→{"Al_2O3_3-ZnSe on QCL at 10μm"},PlotStyle→{Red, Blue,Green}];

Show[B,Frame→True,FrameLabel→{"Wavelength(μm)","Reflectivity(%)"}] ;

Show[%,GridLines→Automatic]

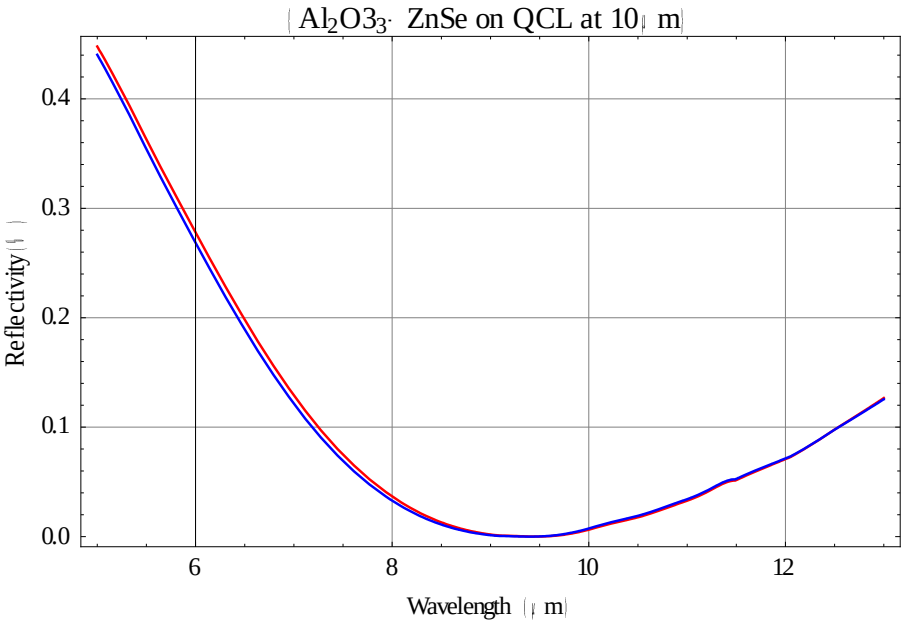

Bibliography

Chakraborty, T., & Apalkov, V. M. (2003). Quantum cascade transitions in nanostructures. *Advances In Physics*, 52(5), 455-521.

Electron Beam Physical Vapor Deposition (2006, December 10). In *Wikipedia, the free* encyclopedia. Retrieved from http://en.wikipedia.org/wiki/Electron_beam_ physical_ vapor_deposition

Faist, J., Capasso, F., Sivco, D., Sirtori, C., Hutchinson, A & Cho, A. Quantum cascade laser. *Science* 264 (1994): 553-556.

Palik, Edward (Ed.). (1997). *Handbook of Optical Constants of Solids, Author and Subject Indices for Volumes II* (pp. 761-775). San Diego: Elsevier Science & Technology.

Gmachl, Claire. Teaching old materials new tricks: Quantum cascade lasers-Band structure-engineering and fun in quantum mechanics. PowerPoint presentation. REU Summer Workshop. 6-7 July 2005.

Hayashi, I. (1984). Heterostructure Lasers. *IEEE Transactions on Electron Devices*, *31*(11), 1630-1642.

Kasap, S. (2006, September 6). Stimulated emission devices LASERS - Developer Zone - National Instruments.*NI Developer Zone*. Retrieved from http://zone.ni. com/devzone/cda/ph/p/id/249

Knight, Randall. D., Jones, Brian & Field, Stuart. (2012). Atoms and molecules. *College physics: a strategic approach* (2nd ed., AP* ed., pp. 980-2). Boston: Pearson.

Maulini, R. "Broadly tunable mid-infrared quantum cascade lasers for spectroscopic applications." Thesis, University of Neuchâtel, Nov. 2006.

Nave, C. R. (n.d.). Semiconductor Concepts. *Hyperphysics*. Retrieved July 20, 2013, from http://hyperphysics.phy-astr.gsu.edu/hbase/solids/semcn.html

Orfanidis, S. (2002, November 1). Reflections and Transmissions. *Electromagnetic Waves and Antennas*. Retrieved from http://www.ece.rutgers.edu/~orfanidi/ ewa/ch05.pdf

Raut, H. K., Ganesh, V. A., Nair, A.S. & Ramakrishna, S. "Anti-reflective coatings: A critical, in-depth review." *Energy and Environmental Science* 4 (2011): 3779-3803.

Spectroscopic Ellipsometry Tutorial - J.A. Woollam Co.. (n.d.).*Spectroscopic Ellipsometers -J.A. Woollam Co.*. Retrieved from http://www.jawoollam.com /tutorial_1.html

Sputter deposition. (2007, October 8). In *Wikipedia, the free encyclopedia*. Retrieved from http://en.wikipedia.org/wiki/Sputter_deposition

Vijayraghavan, K., Jiang, Y., Jang, M., Jiang, A., Choutagunta, K., Vizbaras, A., et al. (2013). Broadly tunable terahertz generation in mid-infrared quantum cascade lasers. *Nature Communications* ,*4:2021*(doi:10.1038). Retrieved from http://users.ece.utexas.edu/~mbelkin/paper

Weida, Miles. http://en.wikipedia.org/wiki/File:QC_Littrow_external_cavity.svg. 26 March 2008.

Williams, Benjamin (2007). Terahertz quantum-cascade lasers. *Nature Photonics* 1.9 517-525.

Yao, Yu, Anthony J. Hoffman, and Claire F. Gmachl (2012). Mid-infrared quantum cascade lasers. *Nature Photonics* 6.7: 432-439.

Vita

Agatha (Kari) Bennett was born in Alice, Texas. She was raised in Guam and the Rio Grande Valley. She received her Bachelors of Science in Biology from UT-Pan American, in Edinburg, Texas. She taught science for five years in Los Fresnos before moving to Central Texas in 1996. She currently resides in Kyle, TX with her husband, Bruce and her daughter, Sydnee. For the past seventeen years, she has taught science at Hays CISD.

Email: bennett_kari@utexas.edu

This paper was typed by the author